

Micro Structural Investigations and Mechanical Properties of Macro Porous Ceramic Materials from Capillary Suspensions

Jens Dittmann,[†] and Norbert Willenbacher

Karlsruhe Institute of Technology, Institute for Mechanical Process Engineering and Mechanics, Gotthard-Franz-Str. 3, Karlsruhe 76131, Germany

Recently, we have introduced a novel, material-independent processing method for producing macro porous ceramics with capillary suspensions as a stable precursor. A capillary suspension is a three-phase system where a small amount of an immiscible secondary liquid is added to a suspension resulting in the formation of a sample spanning particle network. This technology provides open porosities well above 50% and pore sizes ranging from 0.5–100 μm . Here we focus on microstructure formation in the capillary suspensions and its impact on mechanical strength of the corresponding sintered parts. Based on the rheological data and SEM-images, three regimes (I, II, III) are identified with distinctly different flow properties of the wet suspension and characteristic structural features of the sintered ceramic parts depending on the amount of added secondary liquid phase. The average pore size increases and the pore size distribution changes from monomodal (I) to bimodal (II) and broad multimodal (III) with increasing amount of secondary liquid phase. A clear correlation between the yield stress of the wet suspension and the porosity and pore size is observed for regime (I) and (II). Compressive and flexural strength as well as the Young's modulus monotonically decrease with increasing amount of the secondary liquid phase. Absolute values are mainly determined by the porosity and are well predicted by the Gibson & Ashby model for samples corresponding to regime (I) and (II). The broad pore size distribution in regime (III) results in a significantly lower mechanical strength.

I. Introduction

TYPICAL process routes that are used in industry to produce macro porous ceramics are the sacrificial templating, direct foaming, replica techniques, and the partial sintering method.^{1–4} Final sintered properties and the respective processing steps for each process route are listed in Table I.^{1–3,5,6} The most straight forward way to produce macro porous ceramic materials is the partial sintering method. With this method, a powder preparation as suspension or compacted by pressing results in pores <10 μm and porosities up to 50%. Pore size and porosity are determined by the progress of the partial sintering and the particle size of the raw ceramic powder. The other process routes are based on the principle of introducing a space template (solid or gas) into a ceramic preparation. Pores represent then a positive or negative counterpart to the space template at the sintered part obtained by geometrical dimensions and amount of the template. The replica technique is limited because of structural limitations of the impregnated struc-

ture. Using the direct foaming or emulsifying method leads to coalescence of the bubbles or liquid droplets. Small templating particles tend to agglomerate what results in inhomogenous structures.

The process route using capillary suspensions is quite different from the conventional process routes listed above because no template or space holder material is required. Porosity and pore size are the result of a controlled heterogenization of a homogenous green suspension using capillary forces. This results in a lower density of the green body and in that sense improves the approach of partial sintering. Open porosities well above 50% and pore sizes ranging from 0.5–100 μm can be easily achieved.^{7,8} Especially the range of porosities above 50% in combination with pores smaller than 10 μm is hardly accessible with the other techniques mentioned above.

Macroporous sintering materials are widely used as light-weight construction materials, thermal insulators, catalyst carriers, membranes or filters, heat exchangers, and medical implants.^{1,2,4,9} Manufacturing highly porous membranes for sewage filtration from borosilicate glass by the novel capillary suspension technique is work in progress. We also intend to use the porous structure of sintered capillary suspensions for metal matrix composite materials. With this technique the porous structure of a ceramic material is infused with molten metals to combine the properties of ceramic and metal materials in a composite.¹⁰

Capillary suspensions consist of the three-phase system solid–liquid–liquid, in which the two liquid phases are immiscible. Preparing a capillary suspension means to add a small amount of a secondary liquid phase ($\phi_{\text{sec}} \sim 1 \text{ vol}\%$) to a low concentrated pure suspension with a typical particle loading ϕ_{solid} between 5 and 40 vol%. The added secondary liquid phase ϕ_{sec} preferentially wets the solid phase or not and builds up capillary bridges between the particles. The secondary liquid phase preferentially wets the particles if the liquid bulk phase of the pure suspension is displaced from the particle surface by the secondary liquid phase. This process is known from literature as rewetting.¹¹ In the preferentially wetting case (“pendular state”) the three-phase contact angle is $\theta_{\text{SB}} < 90^\circ$. If the secondary liquid is not preferentially wetting (“capillary state”) to the solid, θ_{SB} is $>90^\circ$. In the former case the secondary liquid phase forms capillary liquid bridges among adjacent particles, in the latter case particle clusters are formed entrapping the secondary liquid phase. In both cases the secondary liquid phase droplets are smaller than the dispersed particles. The particles connected by capillary bridges or the clusters including the secondary liquid phase create a sample spanning network which causes a change in the flow behavior. A transition from a liquid to a gel respectively from a weak to a strong gel is observed. In this present work only the better wetting case with $\theta_{\text{SB}} < 90^\circ$ is considered. The strength of a capillary suspension is controlled by the strength of the liquid capillary bridges which is generally orders of magnitude higher than the van-der-Waals attraction among the particles. At

G. Franks—contributing editor

Manuscript No. 34625. Received March 7, 2014; revised June 16, 2014; approved July 24, 2014.

[†]Author to whom correspondence should be addressed. e-mail: jens.dittmann@kit.edu

Table I. Conventional Methods for Producing Macro Porous Ceramics: Typical Pore Sizes $x_{\text{pore,av}}$ and Porosities ε ^{1–3,5,6}

Method	Description	$x_{\text{pore,av}}$ (μm)	ε (%)
Sacrificial templating	(1) Adding of sacrificial phase to ceramic or ceramic precursor in solid or liquid form (2) Drying, pyrolysis or evaporation to remove template (3) Sintering.	1–700	20–90
Direct foaming	(1) Gas incorporation into ceramic suspension or ceramic precursor (2) Setting or drying (3) Sintering	35–1200	40–97
Replica technique	(1) Impregnation or infiltration of a synthetic or natural template by a ceramic suspension or a ceramic precursor (2) Drying or template removal (3) Sintering	10–3000	25–95
Partial sintering	(1) Powder preparation as suspension or compacted by pressing (2) Debinding and sintering or direct sintering	<10	<50

$\phi_{\text{sec}} = \text{const.}$, yield stress σ_y of such suspensions is proportional to the ratio $\Gamma_{\text{SB}}/x_{\text{particle}}$ where Γ_{SB} is the interfacial tension between the two liquid phases and x_{particle} is the average diameter of the dispersed particles.^{12–15} Capillary suspensions are different from pickering emulsions because in pickering emulsions the particles are typically one order of magnitude smaller than the droplets of the added disperse liquid phase and the particles are located at the interface of the two liquids. Furthermore, the pores of sintered parts produced from pickering emulsions are spherical which is usually not true for capillary suspensions.^{4,16}

One unique feature of capillary suspensions is that they can be used as a stable precursor for producing macro porous sintering materials. Porosity and pore size are controlled by the initial solid loading ϕ_{solid} , the median particle diameter x_{particle} and the amount of secondary liquid phase ϕ_{sec} . For $\phi_{\text{sec}} = \text{const.}$, decreasing the fraction of initial solid loading leads to a rise in porosity and decreasing the particle size results in smaller pores. Furthermore, for a constant initial volume fraction of solid and a constant particle size, porosity, and pore size increase with an increasing amount of secondary liquid phase.^{7,8}

After presenting the new capillary suspension concept for making porous ceramic materials in a previous paper we now discuss the mechanical properties of porous ceramics made from capillary suspensions. We demonstrate that the mechanical strength is similar to that of conventional porous ceramics for a given porosity. Furthermore, we discuss the effect of the secondary liquid content on paste rheology as well as structure and mechanical strength of sintered parts.

II. Experimental Procedure

Experiments were carried out using a $\alpha\text{-Al}_2\text{O}_3$ -based model system with paraffin oil as bulk phase and an aqueous sucrose solution as secondary liquid phase. With this material system, principles of the microstructure formation are clearly observable. Furthermore, results from mechanical strength tests of sintered parts can be compared with literature data readily available for porous Al_2O_3 .³

(1) Raw Materials

Paraffin oil with a dynamic viscosity of $\eta = 0.03 \text{ Pa}\cdot\text{s}$ at 20°C and $\alpha\text{-D-sucrose}$ were purchased from Carl Roth (Karlsruhe, Germany) and used as received. The $\alpha\text{-D-sucrose}$ was dissolved in distilled water at 20°C , this solution (1.853M) shows Newtonian flow behavior with a dynamic viscosity of $\eta = 0.08 \text{ Pa}\cdot\text{s}$. Raw $\alpha\text{-Al}_2\text{O}_3$ powders with a density $\rho = 3.94 \text{ g/cm}^3$ and a median particle size of $x_{\text{particle}} = 5.76 \mu\text{m}$ and $x_{\text{particle}} = 1.67 \mu\text{m}$, respectively were

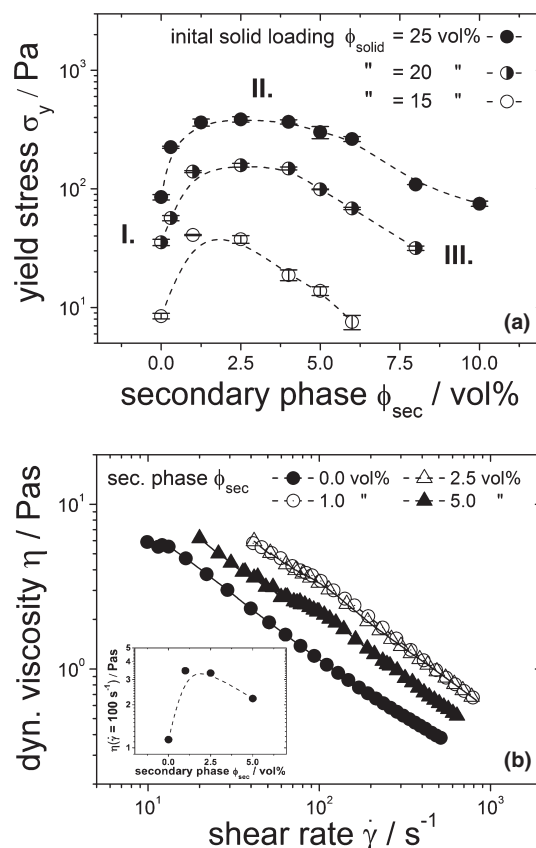


Fig. 1. Yield stress σ_y vs amount of secondary liquid phase ϕ_{sec} for different initial solid loadings ϕ_{solid} (a) dynamic viscosity η vs shear rate $\dot{\gamma}$ and $\eta(\dot{\gamma} = 100 \text{ s}^{-1})$ vs ϕ_{sec} as insert diagram (b) The initial particle size is $x_{\text{particle}} = 1.67 \mu\text{m}$.

donated by Almatix (CT19FG, CT3000SG, Ludwigshafen, Germany). The powder size distribution is in both cases monomodal and narrow. To prevent unwanted agglomeration in the pure suspension, polysorbate-20, a nonionic wetting agent with a hydrophilic–lipophilic balance value of 16.7 from Carl Roth (Tween20, Karlsruhe, Germany) was added as received.

(2) Material Processing

Pure suspensions were prepared by mixing each volume fraction of solid with paraffin oil using a high shear dissolver at 1200 rpm for 20 min followed by a

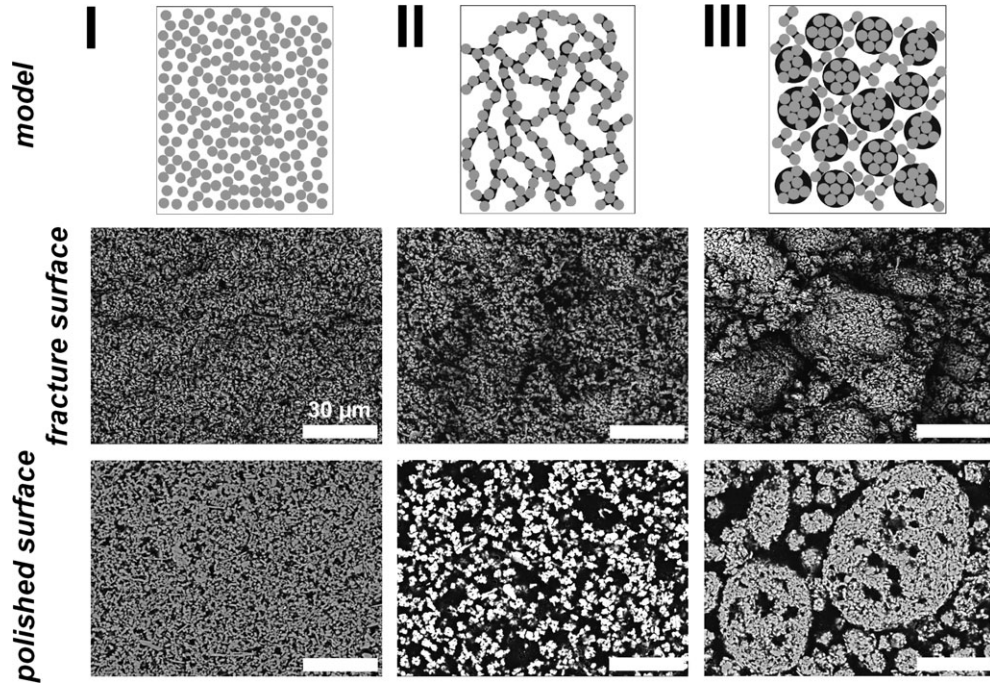


Fig. 2. Three regime model for capillary suspensions at the pendular state with $\theta_{SB} < 90^\circ$, demonstrated for an initial solid loading of $\phi_{solid} = 20$ vol% and an initial particle size $x_{particle} = 5.67$ μm . Shown are the idealized model concept of the wet state and SEM-images of the corresponding fractured and polished surfaces of sintered parts (1650°C, 2 h). Van-der-Waals particle network in regime (I) for $\phi_{sec} = 0.0$ vol%, homogeneous flocculated and sample spanning particle network stabilized with capillary liquid bridges in regime (II) for $\phi_{sec} = 2.5$ vol%, strong aggregation and inhomogeneous structure formation due to the spherical agglomeration in regime (III) for $\phi_{sec} = 8.0$ vol%.

deagglomeration step using a ball mill with 25 mm balls for 24 h at 20°C. The amount of wetting agent was constant for all sample preparations related to the bulk phase. Capillary suspensions were obtained by adding the secondary liquid phase to the pure suspension while stirring with a high shear dissolver at 1000 rpm for 1 min (droplet formation) followed by a second stirring step with a reduced stirring speed of 500 rpm for 1 min (structure formation). So prepared pastes were molded by hand into a sample form (sample size 50 mm \times 10 mm \times 10 mm) and the top face was smoothed using a doctor blade. The sample form was placed on an absorbent pad and directly demolded after spreading. De-binding the bulk phase was carried out by capillary extraction for 5 d at room temperature on the absorbent pad followed by a thermal de-binding procedure at 200°C (30 min), 500°C (1 h), and 800°C (15 min) to ensure a complete and gentle de-binding of the bulk phase and residuals of the sucrose. Samples with $x_{particle} = 5.76$ μm were sintered at 1650°C for 2 h, samples with $x_{particle} = 1.67$ μm were sintered at 1500°C for 1 h.

(3) Characterization

The initial particle size distribution was determined by Fraunhofer diffraction (Helos H0309; Sympatec, Clausthal-Zellerfeld, Germany) using an ultrasonic wet dispersing unit (Quixel, Sympatec) according to DIN EN ISO 8130-13. Yield stress measurements (σ_y) were carried out with a stress-controlled shear rheometer (Thermo Scientific, Mars II, Karlsruhe, Germany) using a vane geometry (Z20 according to DIN 53019-1). Yield stress values were determined from shear stress ramps, according to the tangent method.¹⁷ Three-phase contact angles (θ_{SB}) were calculated using the expanded Young-Dupré-equation.¹² The required interfacial and surface tension data Γ_{SB} , Γ_{Ba} , and Γ_{Sa} were determined using a weight-based tensiometer (Dataphysics, DCAT 11, Filderstadt, Germany) employing a Wilhelmy-plate.¹¹ Contact angles against air (θ_{Ba} , θ_{Sa}) were measured using the sessile-drop method (OCA15, Dataphysics), evaluated by a

numerical Young-Laplace fit of the equation to the droplet shape.¹⁸ The porosity ϵ of the sintered parts was determined from the Archimedes density according to DIN EN 993-1 (calculation of Archimedes density) and DIN EN 993-18 (technical implementation). Mechanical properties were measured following DIN EN 843-1 (flexural strength, σ_f), DIN 51104 (compressive strength, σ_c), and DIN EN 843-2 (Young's modulus, E) using reshaped parts with rectangular cross section. Further, sintered parts were vacuum infused with epoxy resin, mounted on SiC paper and polished with a diamond suspension (Buehler, Düsseldorf, Germany) to obtain crosscut images by scanning-electron-microscopy (SEM-BSE) in backscattering-mode (S-4500; Hitachi, Krefeld, Germany). Pore size distributions $q_3(x_{pore})$ and average pore sizes $x_{pore,av}$ were calculated via image processing using the line intercept count method.¹⁹ Average values are the result of at least three measurements.

III. Results and Discussion

The three-phase contact angle θ_{SB} can be calculated from the surface tensions of the bulk and secondary liquid phase $\Gamma_{Ba} = 30.4 \pm 0.1$ mN/m, $\Gamma_{Sa} = 77.5 \pm 0.1$ mN/m, the interfacial tension between both liquid phases $\Gamma_{SB} = 43.1 \pm 0.2$ mN/m, as well as their contact angles against the solid phase in air $\theta_{Ba} = 0^\circ$, $\theta_{Sa} = 51.8 \pm 0.9^\circ$, respectively. This results in $\theta_{SB} = 66 \pm 1.4^\circ$ confirming that the system is in the pendular state.¹² Errors are the standard deviation from at least three measurements.

(1) Rheological Characterization & Micro Structural Investigations

In the investigation presented here, we have expanded the range of added secondary liquid phase up to $\phi_{sec} = 10$ vol%. Corresponding yield stress σ_y and viscosity $\eta(\dot{\gamma})$ data are shown in Fig. 1. Obviously, σ_y strongly increases with increasing ϕ_{sec} , but then goes through a maximum and finally decreases to the value valid for the suspension without secondary liquid phase [Fig. 1(a)]. The plateau region in

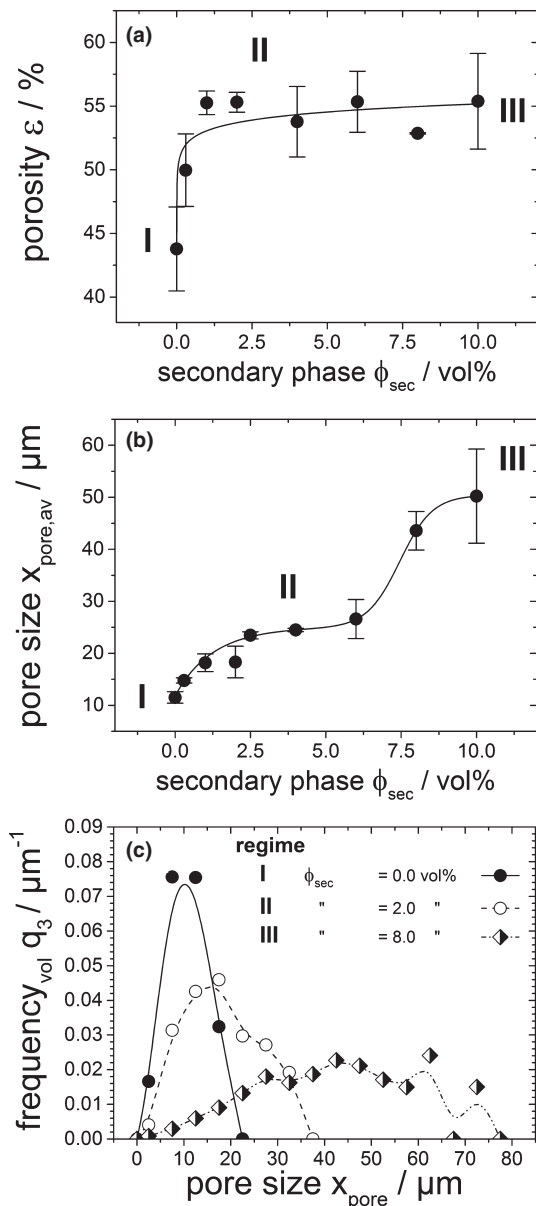


Fig. 3. Porosity ε (a) and average pore size $x_{\text{pore,av}}$ (b) plotted versus the amount of secondary liquid phase ϕ_{sec} and the resulting pore size distributions $q_3(x_{\text{pore}})$ (c) for three different ϕ_{sec} values corresponding to regime (I), (II) and (III). Initial solid loading $\phi_{\text{solid}} = 20$ vol%, $x_{\text{particle}} = 5.67$ μm , sintered at 1650°C for 2 h.

which σ_y exhibits its maximum gets broader with increasing ϕ_{solid} . As shown in Fig. 1(b), the $\eta(\dot{\gamma})$ curves are shifted to the right along the $\dot{\gamma}$ -axis when ϕ_{sec} is increased until a critical value $\phi_{\text{sec,crit}}$ is reached and the shift is less pronounced when ϕ_{sec} is further increased. Accordingly, plotting $\eta(\dot{\gamma} = 100 \text{ s}^{-1})$ vs ϕ_{sec} results in a viscosity maximum [insert Fig. 1(b)]. From the data demonstrated in Fig. 1, we can distinguish three different regimes regarding the effect of ϕ_{sec} on suspension rheology. Anticipating the results presented below we call these regimes (I) structure formation, (II) complete accomplished structure, and (III) structural degradation. To disclose the micro structure corresponding to these three rheological regimes we have removed the liquid phases and prepared sintered parts. Figure 2 displays such SEM-images made from suspensions with $\phi_{\text{solid}} = 20$ vol% but varying amounts of ϕ_{sec} . The images of fractured and the polished surfaces for $\phi_{\text{sec}} = 0$ vol% corresponding to regime (I) show a densely packed, homogeneous distribution of particles. The interaction among particles is dominated by van-der-Waals

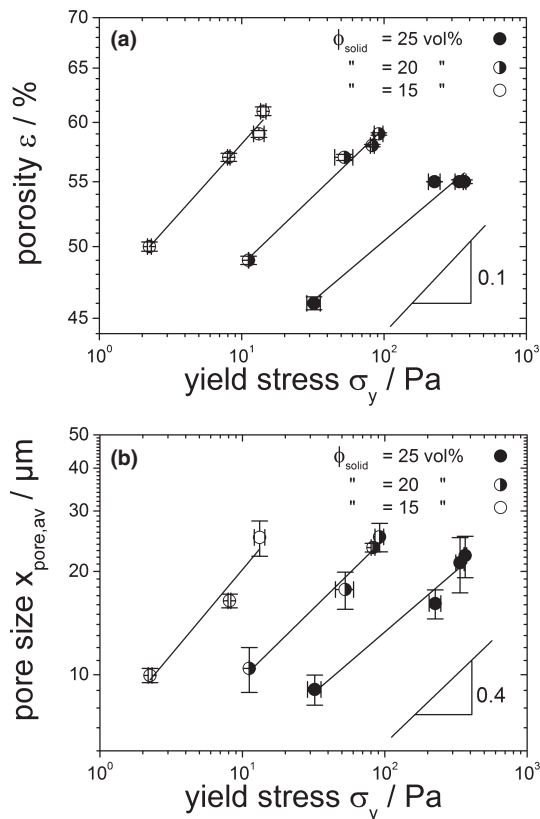


Fig. 4. Porosity ε (a) and average pore size $x_{\text{pore,av}}$ (b) of sintered parts versus yield stress σ_y of the wet pastes. Secondary liquid phase ϕ_{sec} referring to regime (I) and (II), initial particle size of the powder $x_{\text{particle}} = 5.76$ μm , sintered at 1650°C for 2 h.

forces which do not lead to a distinct structure formation. In regime (II) represented here by $\phi_{\text{sec}} = 2.5$ vol%, structure becomes much more open because flocculation is induced by the addition of the secondary liquid phase. This controlled heterogenization of the suspension due to the capillary force between the particles leads to a strong increase of σ_y . At the transition between regime (I) and (II) both states are present because the amount of the secondary liquid phase is not enough to reach all interparticle contact points to built-up capillary liquid bridges. In regime (II), all the particles within the sample volume are connected by capillary liquid bridges thus forming a sample spanning particle network. As ϕ_{sec} increases within regime (II) the capillary liquid bridge volume grows, but obviously σ_y remains constant and accordingly the micro structure also seems to be unaffected. When $\phi_{\text{sec,crit}}$ is exceeded, σ_y decreases and this corresponds for a distinct change in micro structure. The uniformly flocculated structure of regime (II) changes then into a sample spanning network of large compact aggregates in regime (III) with σ_y lower than for a uniformly flocculated network. Formation of these compact aggregates is attributed to the ongoing increase in the liquid bridge volume until the particle contact points are supersaturated. Because of this supersaturation of the particle network, the flocculated structure finally collapses and forms large aggregates with a rising particle coordination number in each aggregate. This phenomenon is already known as spherical agglomeration.²⁰ These aggregates then form a sample spanning aggregate network, with σ_y lower than for a uniformly flocculated network. The critical amount of secondary liquid phase at which the transition from regime (II) to regime (III) occurs, increases with increasing ϕ_{solid} as deduced from the σ_y data shown in Fig. 1(a). This is because more particle-particle contacts have to be saturated before regime (III) is reached when ϕ_{solid} is higher.

(2) Porosity and Pore Size

Figure 3 shows porosity ε , average pore size $x_{\text{pore,av}}$ and pore size distribution $q_3(x_{\text{pore}})$ data for porous sintered parts made from capillary suspensions as described above with an initial solid loading $\phi_{\text{solid}} = 20$ vol%, average particle size $x_{\text{particle}} = 5.76$ μm and various amounts of ϕ_{sec} . The porosity ε [Fig. 3(a)] increases upon addition of the secondary liquid phase to the pure suspension from about 43% in regime (I) to about 55% in regime (II). It remains essentially constant irrespective of ϕ_{sec} even if the critical value $\phi_{\text{sec,crit}}$ at which σ_y and η of the corresponding wet suspension start to decrease and the micro structure of the sintered parts clearly changes is exceeded. The porosity ε of sintered parts made from suspensions corresponding to regime (II) and (III) is essentially equal.

In contrast, the average pore size $x_{\text{pore,av}}$ increases monotonically with increasing amount of the secondary liquid phase [Fig. 3(b)]. The structural regimes (I)–(III) clearly show up these average pore size data. A pore size $x_{\text{pore,av}}$ of about 10 μm is obtained for parts made from the pure suspension [regime (I)] but $x_{\text{pore,av}}$ rises to about 25 μm in regime (II) where the flocculated structure induced by the secondary liquid is present. The formation of large aggregates at high ϕ_{sec} values [regime (III)] results in a further increase of $x_{\text{pore,av}}$ up to about 50 μm at $\phi_{\text{sec}} = 10$ vol%. But not only the average pore size is affected by the structural change, also the pore size distribution q_3 is distinctly different [Fig. 3(c)]. In regime (I) a monomodal pore size distribution is formed, in (II) a second slightly larger characteristic pore size occurs resulting in a bimodal distribution and finally in regime (III) a broad multimodal pore size distribution is found.

As pointed out above, the flow properties of the wet suspensions are directly related to the structure of the corresponding sintered parts. Accordingly, scaling laws relating ε and $x_{\text{pore,av}}$ to σ_y can be established for regime (I) and (II), $\varepsilon \sim \sigma_y^{0.1}$ and $x_{\text{pore,av}} \sim \sigma_y^{0.4}$ are found for all investigated particle loadings as demonstrated in Fig. (4).

(3) Mechanical Properties

We have determined the compressive strength σ_c , flexural strength σ_f , and Young's modulus to characterize the mechanical properties of highly porous sintered parts made from capillary suspensions. In Fig. 5, the mechanical parameters σ_c , σ_f , and E are plotted vs ϕ_{sec} for an initial solid loading $\phi_{\text{solid}} = 20$ vol% and an average particle size $x_{\text{particle}} = 5.76$ μm . In general, σ_c is about 2.6 times higher than the flexural strength σ_f over the whole range of ϕ_{sec} [Fig. 5(a)]. The compressive and flexural strength drop about one order of magnitude upon increasing the amount of ϕ_{sec} from 0.0 to 10.0 vol%. Mechanical properties of highly porous ceramics are mainly controlled by the porosity of the sintered part. For a given chemical composition of the solid material, the mechanical strength of macro porous sintered parts strongly decreases with increasing pore volume fraction.^{21–23} To elucidate whether the mechanical properties of sintered parts made from capillary suspensions depend on porosity ε or average pore size $x_{\text{pore,av}}$, Fig. 5(c) is consulted. This is necessary because with an increasing amount of secondary liquid phase ϕ_{sec} , both porosity ε and pore size $x_{\text{pore,av}}$ are increasing. In Fig. 5(c) compressive strength data from regime (I) and (II) is plotted as a function of $x_{\text{pore,av}}$ for different series of samples with constant ε . It becomes obvious that for constant values of the porosity ε , the compressive strength σ_c is constant, too. But irrespective of $x_{\text{pore,av}}$, an increase of ε results in a decrease of σ_c , as expected. Analogous results are found for the flexural strength σ_f and Young's modulus E . In regime (III) the broadening of the pore size distribution has a strong effect on the mechanical properties, independent of the porosity ε . This leads to significantly lower strength values in regime (III) even if ε is the same as in regime (II).

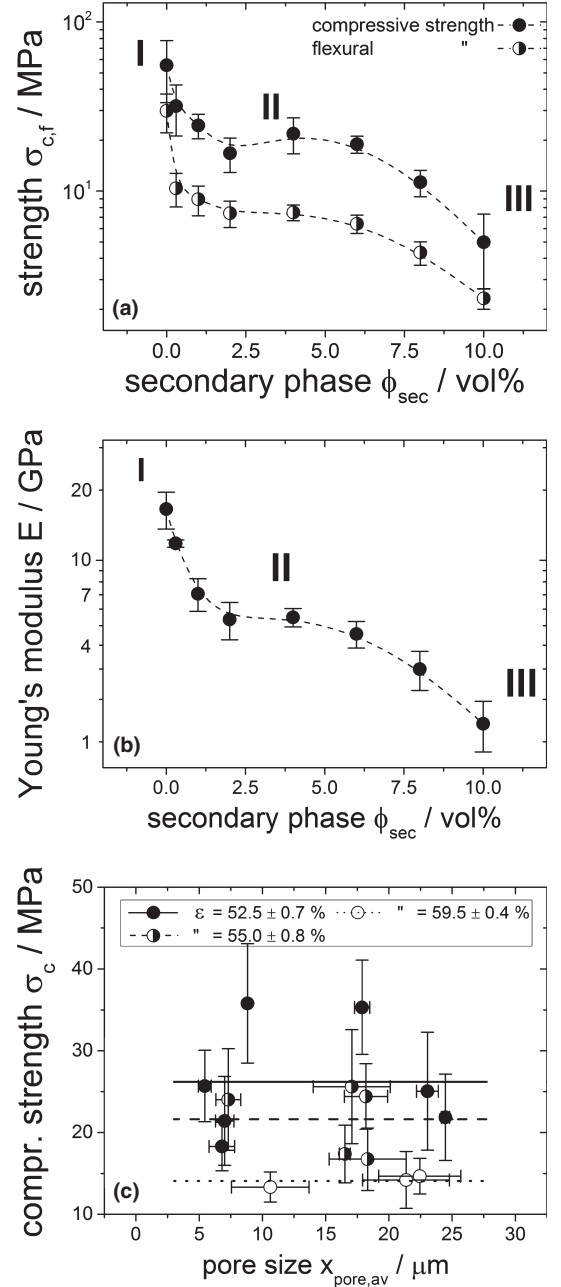


Fig. 5. Compressive and flexural strength $\sigma_{c,f}$ (a) Young's modulus E (b) plotted versus the amount of secondary liquid phase ϕ_{sec} for an initial solid loading of $\phi_{\text{solid}} = 20$ vol%. Compressive strength σ_c vs average pore size $x_{\text{pore,av}}$ for different porosities ε as indicated in the legend (c). Lines in (c) are the average values of the compressive strength at each constant porosity. Initial particle size is $x_{\text{particle}} = 5.67$ μm . Sintered parts have been prepared at 1650°C for 2 h.

Gibson & Ashby have developed a model relating the fracture strength of porous materials to their porosity. Based on the assumption of a uniform cubic cell structure they derive equations for open and closed-cell materials. For the former case they found

$$\frac{\sigma_c}{\sigma_{f,0}} = k_1(1 - \varepsilon)^{k_2} \quad (1)$$

where $\sigma_{f,0}$ is the flexural strength of the dense strut material [$\sigma_{f,0}$ (Al_2O_3) = 400 MPa],²⁴ k_1 is an empirical proportionality constant, and the exponent k_2 depends on the type of material. For brittle materials $k_1 = 0.2$ and $k_2 = 3/2$ is sug-

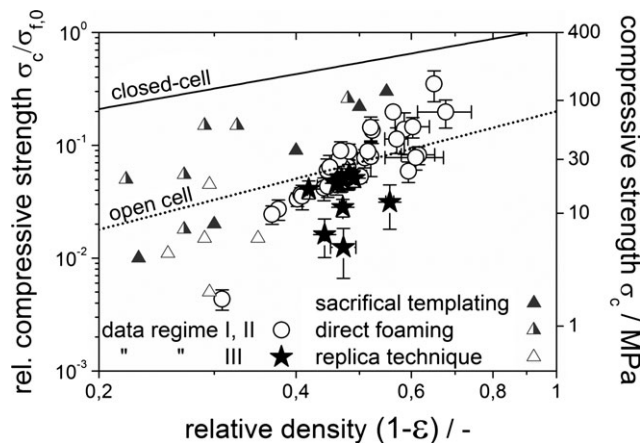


Fig. 6. Relative compressive strength $\sigma_c/\sigma_{f,0}$ and absolute compressive strength σ_c vs relative density $1 - \varepsilon$ where $\sigma_{f,0}$ is the flexural strength of the dense material ($\sigma_{f,0}(\text{Al}_2\text{O}_3) = 400 \text{ MPa}$).²⁴ The solid line represents the closed-cell and the dotted line the open-cell model of Gibson & Ashby for brittle materials.²¹ Results from sintered capillary suspensions (open circles and filled stars) are compared to data from conventional processing routes (filled, half-filled, and open triangles) estimated from literature.³

gested.²¹ Generally, highly porous sintering materials do not show this idealized cubic cell structure. Gauckler and co-workers have analyzed a large set of data covering a wide density range. Results from different processing routes have been compared and also a prefactor $k_1 = 0.2$ was used to provide a good description of this comprehensive set of data.^{3,9} The compressive strength data for the porous sintering materials investigated here are plotted in Fig. 6 as a function of the relative density ($1 - \varepsilon$). As expected, the mechanical strength of the material decreases with an increasing porosity. The absolute values are in good agreement with the model of Gibson & Ashby [Eq. (1) with $k_2 = 3/2$ for brittle materials], using the empirical prefactor with $k_1 = 0.2$ as described in literature. Nevertheless, our data indicate a stronger dependence of the mechanical strength on the relative density than predicted by the model of Gibson & Ashby. Finally, sintered parts from suspensions with high ϕ_{sec} [regime (III)] exhibit a lower mechanical strength than those made from regime (I) and (II) suspensions. According to Gibson & Ashby the pore size is not relevant for the mechanical strength which is only determined by ε . This is true for porous materials made from regime (I) and (II) capillary suspensions as has been shown above in Fig. 5(c). But obviously the broad pore size distribution of materials made from regime (III) suspensions has a significant negative effect on the mechanical strength.

IV. Conclusions

In this article we discuss micro structural and mechanical properties of highly macro porous ceramics produced from capillary suspensions as precursor. The structure of the wet suspensions and the corresponding sintered parts is tightly related and described by a three regime model. In regime (I) of the wet suspension, a van-der-Waals particle network is present. This results in a dense structure at the sintered counterpart. Adding an immiscible secondary liquid phase to the pure suspension, flocculation is induced in regime (II) with the result of a sample spanning particle network, stabilized by capillary liquid bridges. This leads to an opening of the structure with a strong increase in porosity and a characteristic bimodal pore size distribution resulting in a higher average pore size. Increasing the amount of the secondary liquid phase above a critical concentration leads to the formation of large aggregates in regime (III) because of a

supersaturated particle network. Porosity stays constant, but as a result of the strong coarsening of the micro structure, a broad multimodal pore size distribution and a further increase of the average pore size are found. Further, we investigated the mechanical properties of sintered parts. In regime (I) and (II), mechanical strength depends on porosity but not on pore size. Absolute values of compressive strength measured in the present work are well predicted by the Gibson & Ashby model. Increasing the porosity leads to a decrease in mechanical strength, as typically expected for highly porous ceramic materials. In regime (III), mechanical strength of the sintered parts is weaker than for samples with similar porosity made from regime (I) or (II) suspensions. This is attributed to the broad multimodal pore size distribution typically obtained in this regime.

Acknowledgments

We would like to thank the Almatix GmbH for donation of the alumina powder and the smooth collaboration. Further thanks are given to Thomas Lebe for the work at the SEM-microscope and Johannes Maurath for contributing to the mechanical characterization.

References

- Woyansky, C. E. Scott, and W. P. Minnear, "Processing of Porous Ceramics," *Am. Ceram. Soc. Bull.*, **71** [11] 1674–82 (1992).
- Ohji and M. Fukushima, "Macro-Porous Ceramics: Processing and Properties," *Int. Mater. Rev.*, **57** [2] 115–31 (2012).
- A. R. Studart, U. T. Gonzenbach, E. Tervoort, and L. J. Gauckler, "Processing Routes to Macroporous Ceramics: A Review," *J. Am. Ceram. Soc.*, **89** [6] 1771–89 (2006).
- Akartuna, A. R. Studart, E. Tervoort, and L. J. Gauckler, "Macroporous Ceramics from Particle-Stabilized Emulsions," *Adv. Mater.*, **20**, 4717–8 (2008).
- Montanaro, Y. Jorand, G. Fantozzi, and A. Negro, "Ceramic Foams by Powder Processing," *J. Eur. Ceram. Soc.*, **18**, 1339–50 (1998).
- H. Li, J. R. Wijn, P. Layrolle, and K. Groot, "Novel Method to Manufacture Porous Hydroxyapatite by Dual-Phase Mixing," *J. Am. Ceram. Soc.*, **86** [1] 65–72 (2003).
- Dittmann, E. Koos, and N. Willenbacher, "Ceramic Capillary Suspensions: Novel Processing Route for Macroporous Ceramic Materials," *J. Am. Ceram. Soc.*, **96** [2] 391–7 (2013).
- Dittmann, E. Koos, N. Willenbacher, and B. Hochstein, "Process Route for the Production of a Porous Ceramic and Thereby Available Porous Ceramic"; "Verfahren zur Herstellung einer porösen Keramik und damit erhältliche poröse Keramik," German Patent DE 10 2011 106 834, 2011.
- U. T. Gonzenbach, A. R. Studart, E. Tervoort, and L. J. Gauckler, "Macroporous Ceramics from Particle-Stabilized Wet Foams," *J. Am. Ceram. Soc.*, **90** [1] 16–22 (2007).
- Binner, H. Chang, and R. Higginson, "Processing of Ceramic-Metal Interpenetrating Composites," *J. Eur. Ceram. Soc.*, **29**, 837–42 (2009).
- H. D. Dörfler, *Interfaces and Colloid-Disperse Systems: Physics and Chemistry*. Springer, Heidelberg, Berlin, Germany, 2002.
- E. Koos and N. Willenbacher, "Capillary Forces in Suspension Rheology," *Science*, **331**, 897–900 (2011).
- E. Koos, J. Dittmann, and N. Willenbacher, "Capillary Forces in Suspensions: Rheological Properties and Potential Applications," *Kapillarkräfte in Suspensionen: Rheologische Eigenschaften und Potentielle Anwendungen Chem. Ing. Technol.*, **83** [8] 1305–9 (2011).
- E. Koos and N. Willenbacher, "Particle Configurations and Gelation in Capillary Suspensions," *Soft Matter*, **8**, 3988–94 (2012).
- E. Koos, J. Johannsmeier, L. Schwebler, and N. Willenbacher, "Tuning Suspension Rheology Using Capillary Forces," *Soft Matter*, **8**, 6620–8 (2012).
- Akartuna, A. R. Studart, E. Tervoort, U. T. Gonzenbach, and L. J. Gauckler, *Langmuir*, **24**, 7161–8 (2008).
- T. G. Metzger, *The Rheology Handbook*. Vincentz Network, Hannover, Germany, 2011.
- M. M. Bartolotti, M. Brugnara, C. D. Volpe, and S. Siboni, "Numerical Models for the Evaluation of the Contact Angle from Axisymmetric Drop Profiles: A Statistical Comparison," *J. Colloid Interface Sci.*, **336**, 285–97 (2009).
- J. C. Russ and R. T. Dehoff, *Practical Stereology*. Kluwer Academic / Plenum Publishers, New York, NY, 2000.
- H. Takase, "Influence of Interparticle Forces on Selective Wet Agglomeration," *Adv. Powder Technol.*, **20**, 327–34 (2009).
- L. J. Gibson and M. F. Ashby, *Cellular Solids: Structure and Properties*. Cambridge University Press, Cambridge, UK, 1997.
- M. Scheffler and P. Colombo, *Cellular Ceramics: Structure, Manufacturing, Properties and Applications*, Wiley, Weinheim, Germany, 2005.
- Y. B. P. Kwan, "The Porosity Dependence of Flexural Modulus and Strength for Capsule-Free Hot Isostatically Pressed Porous Alumina," *J. Mater. Sci.*, **35**, 1205–11 (2000).
- R. Telle, H. Salang, and H. Scholze, *Keramik*. Springer, Berlin, Heidelberg, Germany, 2007. □